

UCLA

UCLA Previously Published Works

Title

An Overview of Microcrystal Electron Diffraction (MicroED)

Permalink

<https://escholarship.org/uc/item/09f2t96j>

Journal

Annual Review of Biochemistry, 90(1)

ISSN

0066-4154

Authors

Mu, Xuelang
Gillman, Cody
Nguyen, Chi
[et al.](#)

Publication Date

2021-06-20

DOI

10.1146/annurev-biochem-081720-020121

Peer reviewed



Published in final edited form as:

Annu Rev Biochem. 2021 June 20; 90: 431–450. doi:10.1146/annurev-biochem-081720-020121.

An Overview of Microcrystal Electron Diffraction (MicroED)

Xuelang Mu^{1,2,3,*}, Cody Gillman^{1,2,3,*}, Chi Nguyen^{1,*}, Tamir Gonen^{1,2,3}

¹Howard Hughes Medical Institute, Department of Biological Chemistry, University of California, Los Angeles, California 90095, USA

²Molecular Biology Institute, University of California, Los Angeles, California 90095, USA

³Howard Hughes Medical Institute, Department of Physiology, University of California, Los Angeles, California 90095, USA

Abstract

The bedrock of drug discovery and a key tool for understanding cellular function and drug mechanisms of action is the structure determination of chemical compounds, peptides, and proteins. The development of new structure characterization tools, particularly those that fill critical gaps in existing methods, presents important steps forward for structural biology and drug discovery. The emergence of microcrystal electron diffraction (MicroED) expands the application of cryo–electron microscopy to include samples ranging from small molecules and membrane proteins to even large protein complexes using crystals that are one-billionth the size of those required for X-ray crystallography. This review outlines the conception, achievements, and exciting future trajectories for MicroED, an important addition to the existing biophysical toolkit.

Keywords

MicroED; microcrystal electron diffraction; cryo-EM; cryo–electron microscopy; structures; crystallography; proteins

INTRODUCTION

Cryo–electron microscopy (cryo-EM) encompasses techniques that use transmission electron microscopes (TEMs) to extract structural information about cellular, protein, peptide, and chemical specimens (1-3). Since its inception, cryo-EM has provided complementary methods for structure determination of samples that are challenged and in some cases intractable by other structural techniques.

To date, of the nearly 150,000 protein structures deposited in the Protein Data Bank (PDB), 90%, 8%, and 2% were solved by X-ray crystallography, nuclear magnetic resonance (NMR), and cryo-EM, respectively. Despite trailing in the overall number of structures

tgonen@g.ucla.edu .

*These authors contributed equally to this article

DISCLOSURE STATEMENT

The authors are not aware of any affiliations, memberships, funding, or financial holdings that might be perceived as affecting the objectivity of this review.

determined, cryo-EM has experienced a recent surge driven by the advent of improved hardware (4-6), data processing software (7-10), and practices for sample preparation (11). Progress in electron detector technology, in particular, has arguably had the greatest impact on the recent successes in cryo-EM (12). As a result, the number of high-resolution structures determined by TEMs has grown rapidly since the first atomic-resolution cryo-EM protein structure was determined in 2005 (13). Further, since TEM facilities have become much more readily accessible in the last decade, on track to be on the scale of X-ray crystallography, structural biologists around the globe are increasingly becoming equipped to tackle notoriously difficult targets and to push the resolution limits that can be achieved by cryo-EM (14). Owing to this progress, in 2017, for the first time, cryo-EM surpassed NMR for the number of annual entries in the PDB (15).

This review discusses the accomplishments and future directions of the microcrystal electron diffraction (MicroED) cryo-EM technique. MicroED was developed for structure determination of proteins using very small three-dimensional (3D) microcrystals (16). In 2013, Shi et al. demonstrated that a single 3D lysozyme crystal could tolerate more than 90 exposures with limited radiation damage if the exposure to the electron beam was dramatically reduced by two orders of magnitude (16). This seminal study generated the first near-atomic-resolution protein structure from 3D microcrystals using electron diffraction, leading to the birth of MicroED as a distinct branch of the cryo-EM modalities. Since 2013, numerous improvements in the MicroED workflow and technology have been implemented to streamline and democratize the application of MicroED for broader use.

Cryo-EM modalities include single-particle analysis (SPA) (17-19), cryo-electron tomography (cryoET) (20-22), two-dimensional (2D) electron crystallography (23, 24), and, most recently, MicroED (16, 25) (Figure 1). SPA uses high-magnification imaging of purified samples, typically proteins, for the reconstruction of 3D models (26). During SPA, thousands of 2D projection images of ice-embedded particles are captured. Because particles are often positioned in random orientations on the electron microscope (EM) grid, the images can be classified by particle orientation using alignment algorithms (10, 27, 28). The 2D projection averages obtained are then used to reconstruct 3D models (29-31). Since SPA does not require crystallization, this technique is ideal for proteins that resist forming well-ordered crystals, typical of large complexes, flexible, or highly dynamic proteins. Another advantage to SPA is the ability to capture different conformational states of proteins, particularly regions that may have high degree of flexibility (32). There are, however, many challenges intrinsic to SPA, including bottlenecks associated with sample preparation, vitrification, and imaging, that make obtaining high-resolution information difficult. The molecular weight limit is arguably the greatest constraint on SPA. It is still difficult to determine the structures of samples with molecular weights below 40 kDa (33, 34), which is larger than the average size of a protein in the cell.

In cryoET, imaging by TEMs is used to generate models of macromolecules in the context of their native cellular environments (39-42). This technique provides valuable insights into sub-cellular localization and organization of macromolecular complexes (42), in particular those that may be too transient or difficult to capture *in vitro*. The workflow for cryoET is similar to SPA, with a few key differences. Instead of purified proteins, whole

microorganisms or cells are vitrified on EM grids and sliced into thin cross sections using a scanning electron microscope coupled with a focused ion beam (FIB-SEM) (43-45). Images are taken at different tilt angles, aligned, and merged to generate 3D reconstructions of the regions of interest (22, 46, 47). The clear advantage of cryoET is the ability to recapitulate models of macromolecular complexes within the context of their native cellular environment (39-42, 48). The major drawbacks of cryoET are low-throughput workflow and difficulties in achieving high resolution (49). The latter are mainly due to repeated high electron dose exposure required for imaging of a single region, often leading to severe beam-induced radiation damage.

Unlike SPA and cryoET, which depend on imaging, 2D electron crystallography and MicroED take advantage of diffraction. 2D crystallography was developed for membrane proteins that form crystalline lattices in lipid bilayers (50). Using a TEM, 2D crystals are diffracted using a focused electron beam. The diffraction patterns are indexed and merged to create a 3D model (51). The appeal of this technique stems from the opportunity to visualize membrane proteins in environments that mimic cellular membranes (52, 53) and to isolate native 2D crystals directly from cells (23, 54, 55). However, like X-ray crystallography, 2D crystallography is often challenged by laborious optimization assays required to successfully grow 2D crystals, which often require large amounts of highly pure protein (19). Another limitation is that 2D crystals are highly susceptible to radiation damage (2, 17). As such, acquiring a complete data set in 2D electron crystallography often requires diffraction and merging of data from hundreds or even thousands of individual crystals (13, 56, 57).

MicroED was developed as a hybrid method that exploits the advantages of both cryo-EM and X-ray crystallography (16, 58). In MicroED (Figure 2), an electron beam, set at an ultralow dose rate, is used for diffraction of micro- and nanosized 3D crystals (58). During the exposure, the crystal is continuously rotated by the sample stage (25, 59) as the data are recorded as a movie using a fast camera. Each frame in the movie contains a wedge of reciprocal space. As such, MicroED data can be processed using standard X-ray crystallographic software to generate 3D models (60). The main advantage of MicroED is the ability to diffract and extract high-resolution structural information from samples that resist forming large crystals while using significantly less material. Further, whereas X-rays yield only electron density maps (61), electrons, as charged particles, can probe the electrostatic potential of matter (37, 62-64). Thus, MicroED offers users the advantage of mapping the charged, electrostatic states of atoms in structures. As a testament to the power of the technique, to date, all MicroED structures have been determined to relatively high resolution.

With the recent surge of technological improvements introduced to cryo-EM in the last decade, MicroED is becoming an increasingly important tool for structure investigation of proteins and small molecules in drug discovery. To date, there are close to 100 PDB entries reporting MicroED structures. These structures include a rapidly growing number of entries that encompass globular proteins, membrane proteins, protein complexes, peptides, and chemical compounds. The application of faster and more sensitive electron detectors, including direct electron cameras, automated pipelines for data collection and analyses, and

specialized computational methods, is expected to elevate the potential that MicroED holds for transforming the capabilities of cryo-EM.

WORKFLOW

The MicroED workflow has been described in detail (65). Growing protein crystals for MicroED follows the same pipelines as for X-ray crystallography; however, MicroED can extract structural information from crystals that are one-billionth the size required for X-ray diffraction (58). The initial identification of microcrystals for MicroED, however, requires practice as they are difficult to visualize under light microscopes (66). To remedy this hurdle, microcrystals can be identified in crystallization drop experiments using alternative detection methods, including ultraviolet (UV) fluorescence, second-order nonlinear imaging of chiral crystals (SONICC) (67), fluorescence microscopy, and negative-stain electron microscopy (68). Crystallization drops that appear cloudy, which are ordinarily considered failed crystallization experiments for X-ray diffraction, should be carefully inspected, as small micro- and nanometer-sized crystals may be present (63). One should note that some drops with protein precipitates do not contain microcrystals, and false positives can be detected by UV. For instance, protein aggregates may appear as crystalline puncta when exposed to UV light. Further, selective detergents used for solubilization of membrane proteins can also fluoresce under UV.

Once microcrystals have been obtained, the crystal solution is applied to a glow-discharged EM grid, blotted to remove excess solution, and cryo-cooled by plunging into liquid ethane (60). For anhydrous samples, typically small molecules or natural products, the crystals, often as powder, are applied directly to EM grids (69) and analyzed under cryogenic conditions (58) to minimize radiation damage (70). In some cases where the samples are robust, MicroED analysis can be conducted without cooling (71). When larger 1–5 μm crystals form, sizes that are still challenging for traditional X-ray crystallography but too big for MicroED, fragmentation methods (72) or FIB-SEM can be used to generate smaller crystals for electron diffraction (73-76).

Once the crystals are applied to the grid, the grids are then loaded onto the TEM under cryogenic conditions for data acquisition. The grids are typically surveyed in bright-field mode or overfocused diffraction to assess overall ice thickness and to identify areas that contain crystals of appropriate sizes (25). Once crystals are located, a test diffraction pattern is recorded to assess crystal quality. This step can be achieved using automated software such as serial EM (25). If high-quality diffraction is observed, a data set is recorded on a fast camera as a movie with the electron dose rate (exposure) set to 0.01–0.05 $\text{e}^- \text{\AA}^{-2} \text{s}^{-1}$ while the crystal is continuously rotated on the sample stage (25, 60). The exposure used in MicroED is ~100 times lower than what is used for other cryo-EM modalities and significantly reduces radiation damage. Continuous rotation of the sample in MicroED improves the accuracy of the reflection intensities and reduces the effects of dynamical scattering (16, 25, 60, 77), a strategy that leads to data sets that are consistently superior to those prepared by still-diffraction.

Continuous rotation of the crystal at a fixed speed during diffraction in MicroED is analogous to the rotation method used in X-ray crystallography, where individual frames in the MicroED movie contain a wedge of the reciprocal space (25, 78). Thus, MicroED data can be directly processed using standard X-ray crystallographic software (76, 78). MicroED data have been successfully indexed, integrated, and scaled using standard X-ray crystallography software, including XDS (79), iMOSFLM (80), DIALS (81), SHELX (82), and HKL2000 (78). High-resolution (better than ~ 1.2 Å) data sets are required for solving structures by ab initio methods (82). As such, historically, the majority of protein structures solved by MicroED have depended on molecular replacement to solve the phase problem, which is contingent on the availability of search models with high structural homology (83). Recent breakthroughs in phasing strategies include the use of imaging (84-87), fragment-based phase extension (37), ARCIMBOLDO (88), and radiation damage (89).

ADVANTAGES AND APPLICATION OF MICROCRYSTALS FOR MicroED

The growth of large and well-ordered single crystals suitable for X-ray diffraction analysis is a major rate-limiting step for structure determination of proteins (90), especially those that are integral to membranes or that form complexes. Quality biochemical preparation of protein samples is essential for all structural characterization. This includes determining the conditions required to obtain highly pure and stable proteins or their complexes. Because electrons interact with matter more strongly than X-rays, and those interactions result in more useful elastic scattering events (66), the crystals required for MicroED can often be one-billionth the size of those needed for X-ray diffraction. As such, MicroED fills an important gap in biophysics to enable structure elucidation from samples that may not be tractable by other methods.

Small crystals, those that can be used for MicroED, offer several advantages over larger crystals. Small crystals are typically much easier to obtain than larger ones, which also often suffer from more detrimental pathologies such as twinning and multiple and/or mosaic lattices (72, 91). Smaller crystals suffer fewer long-range defects and tend to be better ordered (50). Comparative analysis of eight different samples using both X-ray and MicroED found that smaller crystal fragments resulted in higher-resolution data than the larger parent crystals (72). Moreover, there is no need to include cryoprotectants, a customary practice in X-ray crystallography, because the crystals for MicroED are rapidly vitrified. A recent study also demonstrated that soaking ligands into small crystals is more efficient than for larger crystals, a phenomenon that sets the stage for high-throughput drug discovery by MicroED (92).

The advantages offered by small crystals have expanded the application of MicroED to the study of small organic and inorganic molecules as well as peptides and natural products (16, 56, 57, 93, 94). Between 2016 and 2018, MicroED made important leaps in determining the structure of small molecules from powders instead of grown crystals (58, 69, 91, 95), and directly from mixtures (69). Chemical compounds often crystallize as multiple different lattices, referred to as polymorphs. The presence of multiple crystal lattices in a single experiment, particularly those in mixtures, has posed major hurdles for structure characterization by X-ray diffraction (94). In sharp contrast, MicroED was

able to obtain distinct structures from a mixture of powders containing several different small molecules and natural products (25). In these studies, hydrogen atoms of the small molecules, including carbamazepine, prescribed today for the treatment of convulsive and bipolar diseases (96, 97), were resolved (Figure 3). Many other structures of small molecules have been reported by MicroED recently, including Grippostad (94), an antiviral drug for the treatment of the common cold and the flu (98), and a recent example of the nonfullerene acceptor semiconductive material ITIC-Th (Figure 3).

While nanocrystals, smaller than ~500 nm, are ideal for MicroED, thicker crystals (that are still too small for X-ray) can also be optimized for MicroED. Large crystals can be trimmed to appropriate sizes for MicroED by mechanical fragmentation methods (72) or by using a FIB-SEM (73-76). Several mechanical fragmentation approaches have been applied to prepare large crystals for MicroED, including sonication, vigorous pipetting, and vortexing (72). Generally, the gentler fragmentation through pipetting is better for fragile samples, while harsher methods, such as vortexing and sonication, are needed to break more robust crystals. As proof of principle, eight proteins including lysozyme, xylanase, thaumatin, trypsin, proteinase K, thermolysin, transforming growth factor beta paired type II complex (TGF- β m:T β RII), and a segment of the tau protein—with molecular weights ranging from 0.7 to 34.6 kDa and solvent contents between 30% and 60% were fragmented and their structures determined by MicroED (72). The first six of these proteins are standard model systems. The last two are nonstandard specimens that formed large, imperfect crystals. In all examples, the large crystals were fragmented by one of the three mechanical methods mentioned above before transferring onto EM grids for MicroED. The distribution of micrometer- or nanometer-sized crystal fragments on the EM grid was relatively uniform, and single-crystal data sets were collected by continuous rotation. The standard samples obtained by MicroED are comparable or, in some cases, higher in resolution than those obtained by X-ray diffraction (72). For the two nonstandard samples, the resolution obtained from fragmented crystallites was better than the resolution of the parent crystals and, in one case, the resolution of the structure improved from 8 Å in X-ray to ~ 1 Å with MicroED. These results suggest that mechanical fragmentation itself does not lead to additional damage to the crystal lattice and instead is a viable method for sample preparation for structure determination by MicroED.

In addition to fragmentation, FIB-milling of frozen protein crystals is another approach to trim large crystals for MicroED. During this process, the FIB is used to mill away and remove excess material from the crystal to generate lamellae with appropriate thickness for MicroED (73-76, 99) (Figure 4). During FIB-mill, precoating with a thin layer of platinum is used to protect the specimens (73). Platinum coating can also enhance the physical stability of the grid, functioning as a protective layer above the specimen. Cryo-FIB-milling of lysozyme crystals has been shown to preserve the internal structure of trimmed lamellae and maintain high-resolution diffraction capacity. In combination with MicroED, FIB-milled lamellae of crystals generated a 1.9 Å resolution structure of lysozyme (73). To further push the boundaries of samples that could be used for structure determination by FIB-mill and -MicroED, new crystal “polishing” protocols were established (75). Using proteinase K as a model system, a lower-current ion beam was used as a final polishing step to trim away flanking regions of lamellae. Because the final FIB current used was lower, the amount

of radiation decay was reduced in the resulting lamellae. This strategy was successful in improving the resolution of the proteinase K crystal lamellae to 1.79 Å (75). Fragmentation and milling widen the application range of crystal sizes suitable for MicroED without further additional optimization steps required for generating and screening for smaller crystals.

Structures of proteins bound with small-molecule ligands provide important information about the mechanism of action, insights that are vital for dissecting protein function to lay the groundwork for drug discovery and development (discussed further below). These protein–ligand crystal complexes are generated by either cocrystallizing the protein with the ligands or soaking ligands into preformed protein crystals (99). Here MicroED offers another advantage because diffusion of small molecules is more efficient into small rather than into large crystals (100). A recent study demonstrated that simply soaking small molecules into preformed proteinase K microcrystals on the TEM grid was sufficient to yield a high-resolution structure where several ligands were observed at high occupancy (92). Thus, combining ligand-soaked crystals with MicroED offers strategies to improve the current drug discovery pipeline.

A Robust Method for Structure Determination Using Single 3D Nanocrystals

The very first novel protein structure determined by electron diffraction from 3D crystals was that of the water channel aquaporin-0 (13, 101). Although referred to as 2D crystals in the publication, the very thin crystals had two layers, officially making them 3D crystals. Electron diffraction data were collected from thousands of crystals. Of those, data from more than 200 crystals were integrated and merged to yield a fully refined structure at the atomic resolution of 1.9 Å in 2005 (13). Additional examples of crystal samples that were referred to as 2D but were actually 3D include aquaporin-4 (85) and the gap junction connexin 26 (102), which formed two- and six-layer crystals, respectively. In these studies, the electron diffraction data were phased using image data (13, 85, 103, 104). In 2013, MicroED established robust, streamlined methods for the collection of data using single 3D nanocrystals. In 2015, the first novel structure was determined by continuous-rotation MicroED: that of the amyloid structure of α -synuclein NACore (66) (Figure 5a), a hallmark of Parkinson's disease (105).

The α -synuclein NACore resisted structure determination for more than 10 years because large crystals could not be obtained. The α -synuclein NACore microcrystals used for MicroED were invisible by light microscopy and not suitable for X-ray diffraction studies. These tiny crystals, however, yielded an atomic, 1.4 Å resolution structure of α -synuclein NACore by MicroED, enabling the observation of protons by cryo-EM (66). The structures of another four prion peptides from Sup35 prion were also determined by MicroED at 1 Å resolution in 2016 (91). The high resolutions achieved in these studies allowed *ab initio* structure determination by direct methods (discussed below).

Membrane proteins that are crystallized in detergent micelles, bicelles, or lipid cubic phases often have fewer crystal contact sites than soluble proteins. As such, membrane proteins are especially fragile and tend to grow small crystals that diffract poorly by X-ray. In 2015, MicroED was successfully applied to determine a 3.4 Å resolution structure of the membrane protein Ca⁺ ATPase using ultrathin 3D protein crystals (64) (Figure 5b).

Importantly, the Coulomb potential maps that were generated by MicroED contained unique information about the charged states of amino acid residues, cofactors, and ligands. Further, in 2018, the structure of the nonselective cation channel NaK (Figure 5b) was captured in two new conformations by MicroED (63). Because MicroED can be used to gauge the charge states of chemical moieties in structures, several sodium ions were identified inside the channel pore. A new transient state in which a partially hydrated sodium ion occupied the entrance to the channel selectivity filter was also captured. Together, these studies illustrate the capacity of MicroED to investigate dynamics and Coulomb potential in membrane protein structures.

In addition to membrane proteins, MicroED has also successfully determined the structure of TGF- β m:T β RII (103). This complex formed large but poorly ordered crystals, posing considerable challenges for X-ray crystallography. Breaking these crystals into fragments produced well-diffracting microcrystals (discussed above) that yielded diffraction data at atomic resolution (Figure 5c).

MicroED IN DRUG DISCOVERY

The challenges in structural characterization of proteins, as well as ligands and protein–ligand complexes, present major bottlenecks in rational drug design and development. In the short time since its conception, MicroED has already contributed to drug discovery efforts through structure determination of protein–ligand complexes and supramolecular resolution (better than ~ 1 Å resolution) of bioactive small molecules and natural products. The very first drug discovery study using MicroED was that of the homohexameric HIV GAG capsid protein in complex with the viral maturation inhibitor bevirimat (104). HIV GAG is a structural protein required for the budding of mature, infectious viral particles from host cells (106) (Figure 6). Before the release of the viral particles, the GAG proteins must be processed through proteolytic cleavage by HIV proteases at several sites (107). Bevirimat is a small-molecule ligand that binds directly to and blocks proteolytic processing of GAG (108). The unprocessed and uncleaved GAG protein results in the release of immature and noninfectious HIV particles (108). Although bevirimat reached Phase IIb clinical trials, it was never fully developed into a marketed therapeutic because of low efficacy and the fact that many patients were unresponsive to the drug. At the time, the bevirimat mechanism of action was unknown, abrogating efforts to reengineer this drug for its full therapeutic potential. To better understand the mechanism of action, the structure of HIV GAG in complex with bevirimat has been pursued by X-ray crystallography. Efforts to determine the structure of the GAG–bevirimat complex by both cocrystallization and ligand soaking failed to produce crystals amenable to X-ray diffraction. Ultimately, coupling time-resolved studies with MicroED allowed for structure determination of this elusive complex. To obtain MicroED data of the complex, bevirimat was added to GAG crystals on EM grids and immediately frozen in liquid ethane. This strategy allowed for rapid diffusion of the ligand into the crystals (see the section titled Advantages and Application of Microcrystals for MicroED) while preserving the structural integrity of the GAG microcrystals (104) (Figure 6a). The protein–ligand MicroED structure revealed the binding site of the drug, wedged in the sixfold axis of the GAG hexamer where bevirimat acts as an allosteric inhibitor to prevent processing by proteases, trapping the immature form of HIV (104) (Figure 6b).

This MicroED structure revealed the bevirimat mechanism of action, laying the groundwork for chemical modifications of the ligand to tune the bioactivity of derivatives for future therapeutic application.

Although MicroED was originally developed for studying protein assemblies (16, 38), it rapidly expanded as a powerful tool for structural characterization of small molecules and natural products. One of the first MicroED structures of a small-molecule drug was that of carbamazepine in 2016 to 1 Å resolution (95) (Figure 3). Importantly, the *ab initio* carbamazepine structure was the first to demonstrate that MicroED data can be obtained from samples prepared under anhydrous conditions, at room temperature, using continuous rotation, and with phases solved by direct methods. These new developments expanded the application of MicroED for structure determination of chemical compounds by circumventing the challenging and, often, laborious steps involved in the preparation of hydrated samples under cryogenic conditions (66). In 2018, the structure of frozen and hydrated carbamazepine was determined using a breakthrough method for grid preparation where powders instead of grown crystals were used for MicroED (69).

Under cryogenic conditions, the MicroED structure of carbamazepine was determined at a higher resolution than in the room temperature study, and all hydrogen atoms were identified in 2018. Later in 2018, the structures of 12 different small molecules (69) as well as MBBF₄ (94), a methylene blue derivative with numerous medical applications including its activity as a photo-activatable antimicrobial agent (109), were solved, further solidifying the capabilities of continuous rotation MicroED for small-molecule structure determination (58) (Figure 3).

Unlike small molecules, biosynthesized natural products are typically larger, structurally dynamic, obtained in small quantities, and difficult to crystallize, posing considerable challenges for X-ray studies. When natural products do crystallize, these crystals are often too small and do not yield structures by X-ray diffraction (110, 111). Using the powder-to-structure pipeline (69), MicroED determined the structure of brucine (Figure 7), an alkaloid toxin with anticancer properties (112). The MicroED structure of brucine at 0.9 Å resolution allowed for the definitive assignment of its chiral centers, key for understanding its toxicity and anticancer properties (58). Relative to brucine, amino acid-derived natural products called ribosomally synthesized and post-translationally modified peptides (RiPPs) are large, reaching several kilodaltons in size (113). Two examples of RiPP natural products with structures determined by MicroED include 3-thiaGlu (110) and thiostrepton (114) (Figure 7). Thiostrepton is a RiPP antibiotic currently used in veterinary medicine (114). Although thiostrepton has been studied by NMR (110) and X-ray crystallography (115), the ease of its characterization by the powder-to-structure pipeline speaks to the robustness of MicroED for structural characterization of large, flexible natural products (Figure 7).

Genome analysis of the plant pathogen *Pseudomonas syringae* pv. *maculicola* revealed a gene cluster encoding an unusual combination of biosynthetic enzymes that produces an unknown natural product (110). Analysis of the biosynthetic enzymes revealed that, unlike other RiPPs, biosynthesis of the final natural product, later called 3-thiaGlu (Figure 7), involves the extension of the peptide in an ATP- and amino acyl-tRNA-dependent manner,

instead of the canonical scheme via the ribosome (110). Completion of the biosynthesis of 3-thiaGlu also requires several additional steps, including proteolysis of a terminal cysteine for installation of the glutamylated thiol group, a peptide modification that blocks jasmonate and ethylene signaling pathways (116). Despite considerable effort, X-ray crystallography failed to generate a structure of 3-thiaGlu. Using nanocrystals, MicroED readily provided a 0.9 Å resolution of the 3-thiaGlu peptide (PDB identifier: 6PO6) (110), allowing assignment of its chiral centers and providing further evidence for the proposed biosynthetic scheme.

The structures of 3-methyloxindole and 1-methyl-2-indanone (Figure 7), like that of 3-thiaGlu, were difficult to obtain and were finally solved by applying MicroED (111). These non-canonical amino acids are products from the condensation of 3-substituted oxindoles and L-serine, a reaction catalyzed by a TrpB enzyme engineered through directed evolution. The MicroED structure of the 3-methyloxindole and 1-methyl-2-indanone products from the engineered TrpB provided evidence of the newly installed *S*-configuration at the γ carbon, broadening the application of the enzyme for asymmetric catalysis. Here, the structures of these amino acids obtained by MicroED were used to inform biosynthetic pathways for green chemistry.

Thus far, MicroED still requires internal markers to determine the absolute configuration of chemical compounds (110, 111). An internal marker, such as a naturally occurring L amino acid, is typically incorporated and used to deduce the relative configuration of all other centers in natural products and small molecules. Moving forward, the development of strategies for determining the absolute configurations of chemical compounds without the use of internal markers would widen the application of MicroED for drug discovery.

OVERCOMING RADIATION DAMAGE IN MicroED

Radiation damage remains a major obstacle for structural studies, leading to reduced resolution, poor map quality, and structural damage caused by bond breakage and even gross morphological decay (117). For protein X-ray crystallography, the first study that addressed radiation damage dates back to 1962, when Blake & Phillips (118) measured the loss in intensities of reflections as a function of time of X-ray exposure. Several subsequent studies, including those by Hendrickson (119), moved the field from room-temperature to cryogenic data collection to minimize the effects of radiation damage.

Radiation damage can be subcategorized into two forms: global and site specific. Global radiation damage typically results from the disruption of the crystal lattice, which decreases the intensities of diffraction patterns. This phenomenon can be detected during data processing when changes in unit cell dimensions (120) and increases in B-factors are observed (121). In contrast, site-specific radiation damage is not uniform, accumulates at certain chemical moieties, is not typically detected during data processing, and is observable only during an examination of the real-space map (122). For both global and site-specific radiation damage, the degree of sample decay depends on, among other things, the composition of the sample and the surrounding solution, and is proportional to the amount of energy used (120-122).

In the model system of proteinase K, both global and site-specific radiation damage have been examined for MicroED (70). These studies illustrate that increased electron dosage (from $1.1 \text{ e}^- \text{ \AA}^{-2}$ to $3.1 \text{ e}^- \text{ \AA}^{-2}$) resulted in greater loss of detectable reflections in higher-resolution shells of MicroED data (70) (Figure 8a). The higher exposures during MicroED experiments also resulted in increases in unit cell dimensions and B-factors, both indicators of global radiation damage (Figure 8b). Similarly, higher exposures also led to greater site-specific radiation damage that accumulated on specific amino acids, including glutamic acid, aspartic acid, and cysteines, suggesting that radiation damage in MicroED follows trends similar to radiation damage in X-ray crystallography (Figure 8c). To curb the effects of radiation damage, samples are often vitrified (123). However, even with the combination of vitrification, continuous-rotation data collection, and exposure to extremely low doses of electrons ($0.01 \text{ e}^- \text{ \AA}^{-2} \text{ s}^{-1}$), samples can still suffer from radiation damage during MicroED experiments (70). Recent studies suggest that using a faster and more sensitive camera, the direct electron detector Falcon III, is a strategy to further mitigate radiation damage for MicroED experiments (110, 111, 124) (Figure 9).

SOLVING THE PHASE PROBLEM IN MicroED

In MicroED experiments, as with X-ray diffraction, phases are lost—a challenge referred to in both techniques as the phase problem (125). For both MicroED and X-ray crystallography, the phases can be recovered by molecular replacement and ab initio direct methods (58, 66). While molecular replacement is dependent on topological similarities between the search models and the structures to be determined (126), direct methods require crystals that diffract to fairly high resolution, $\sim 1 \text{ \AA}$ or better (127). The PDB contains 150,000 deposited structures, many of which share conserved protein folds. Due to the conservation of folds across families of proteins, molecular replacement is currently used to calculate phases for roughly 90% of structures deposited to the PDB. Anomalous methods (125) that are prevalent in X-ray crystallography are not possible in MicroED due to the very short wavelengths of electrons (89).

For MicroED, several methods have been successful in solving the phase problem. These include the use of image data (84-87), ab initio structure determination (91), and radiation-induced damage for phasing (RIP) (89). During RIP, a single data set from the sample crystal is split into two (128). The first part of the data set consists of earlier frames that contain less accumulated radiation damage. The second set of frames comprises data that were collected after the first set and consequently has accumulated more radiation damage (128). Using a method similar to isomorphous replacement (129), the two halved sub-data sets are subtracted from one another to generate a difference data set. The difference data set is then used to identify focal points of specific radiation-damaged, such as the hydrolysis of disulfide bonds or ionized metals. Because exposure to electron beams, even at low dosages, can lead to radiation damage during diffraction studies (70), RIP is a promising strategy for obtaining experimental phases for MicroED experiments.

To test if experimental phasing using RIP is a viable strategy for determining novel MicroED structures, the previously solved structure of the prion heptapeptide corresponding to the GSNQNNF sequence was used as a model system (89). To maximize completeness,

11 crystals of the heptapeptide were used to collect two data sets: one with the exposure of $0.17 \text{ e}^- \text{ \AA}^{-2}$ and the second at $0.5 \text{ e}^- \text{ \AA}^{-2}$. The structure amplitudes of the low-dose data set were subtracted from the high-dose data set to calculate a difference data set. The difference was used to calculate a difference Patterson map to identify the location of radiation damage resulting from higher doses of electrons (89). This strategy identified a single solution corresponding to a zinc atom (Figure 10a). The zinc position was then used to calculate the initial phases to generate a density map for model building of the peptide structure (89) (Figure 10b-d).

In summary, MicroED is a relatively young field of study within cryo-EM. In less than a decade since the conception of the technique (16), more than 100 MicroED structures have been determined for proteins, protein complexes, natural products, peptides, and small organic and inorganic molecules. As the method continues to be improved with better hardware, automation, and software, the usefulness and broad applicability of MicroED will only increase.

ACKNOWLEDGMENTS

This study was supported by the National Institutes of Health grant P41GM136508. The Gonen laboratory is supported by funds from the Howard Hughes Medical Institute.

LITERATURE CITED

1. Dubochet J, Booyl FP, Freeman R, Jones AV, Walter CA. 1981. Low temperature electron microscopy. *Ann. Rev. Biophys* 10:133–49
2. Taylor KA, Glaeser RM. 1974. Electron diffraction of frozen, hydrated protein crystals. *Science* 186:1036–37 [PubMed: 4469695]
3. Wang L, Sigworth FJ. 2006. Cryo-EM and single particles. *Physiology* 21:13–18 [PubMed: 16443818]
4. Bai XC, Fernandez IS, McMullan G, Scheres SHW. 2013. Ribosome structures to near-atomic resolution from thirty thousand cryo-EM particles. *eLife* 2:e00461 [PubMed: 23427024]
5. Herzik MA, Wu M, Lander GC. 2017. Achieving better-than-3-Å resolution by single-particle cryo-EM at 200 keV. *Nat. Methods* 14:1075–78 [PubMed: 28991891]
6. Myasnikov A, Zheng S, Bulkley D, Cheng Y, Agard D. 2018. K3—A first look at the new direct electron detection camera from Gatan Company. *Microsc. Microanal* 24:890–91
7. Punjani A, Rubinstein JL, Fleet DJ, Brubaker MA. 2017. CryoSPARC: algorithms for rapid unsupervised cryo-EM structure determination. *Nat. Methods* 14:290–96 [PubMed: 28165473]
8. Tegunov D, Cramer P. 2019. Real-time cryo-electron microscopy data preprocessing with Warp. *Nat. Methods* 16:1146–52 [PubMed: 31591575]
9. Wagner T, Merino F, Stabrin M, Moriya T, Antoni C, et al. 2019. SPHIRE-crYOLO is a fast and accurate fully automated particle picker for cryo-EM. *Commun. Biol* 2:218 [PubMed: 31240256]
10. Zivanov J, Nakane T, Forsberg BO, Kimanius D, Hagen WJH, et al. 2018. New tools for automated high-resolution cryo-EM structure determination in RELION-3. *eLife* 7:e42166 [PubMed: 30412051]
11. Thompson RF, Walker M, Siebert CA, Muench SP, Ranson NA. 2016. An introduction to sample preparation and imaging by cryo-electron microscopy for structural biology. *Methods* 100:3–15 [PubMed: 26931652]
12. McMullan G, Faruqi AR, Henderson R. 2016. Direct electron detectors. *Methods Enzymol.* 579:1–17 [PubMed: 27572721]
13. Gonen T, Cheng Y, Sliz P, Hiroaki Y, Fujiyoshi Y, et al. 2005. Lipid-protein interactions in double-layered two-dimensional AQP0 crystals. *Nature* 438:633–38 [PubMed: 16319884]

14. Subramanian R, Mayor S, Vinothkumar KR. 2019. The resolution revolution reaches India. *Biophys. Rev* 11:513–14 [PubMed: 31267327]
15. Susannah S, Ando N. 2018. X-rays in the cryo-EM era: structural biology's dynamic future. *Biochemistry* 57:277–85 [PubMed: 29227642]
16. Shi D, Nannenga BL, Iadanza MG, Gonen T. 2013. Three-dimensional electron crystallography of protein microcrystals. *eLife* 2:e01345 [PubMed: 24252878]
17. Dubochet J, Adrian M, Chang JJ, Homo JC, Lepault J, et al. 1988. Cryo-electron microscopy of vitrified specimens. *Q. Rev. Biophys* 21:129–228 [PubMed: 3043536]
18. Taylor DW, Zhu Y, Staals RHJ, Kornfeld JE, Shinkai A, et al. 2015. Structures of the CRISPR-Cmr complex reveal mode of RNA target positioning. *Science* 348:581–86 [PubMed: 25837515]
19. Cheng Y 2018. Single-particle cryo-EM—How did it get here and where will it go. *Science* 361:876–80 [PubMed: 30166484]
20. Murphy GE, Jensen GJ. 2005. Electron cryotomography of the *E. coli* pyruvate and 2-oxoglutarate dehydrogenase complexes. *Structure* 13:1765–73 [PubMed: 16338405]
21. Komeili A, Li Z, Newman DK, Jensen GJ. 2006. Magnetosomes are cell membrane invaginations organized by the actin-like protein MamK. *Science* 311:242–46 [PubMed: 16373532]
22. Oikonomou CM, Jensen GJ. 2017. Cellular electron cryotomography: toward structural biology in situ. *Annu. Rev. Biochem* 86:873–96 [PubMed: 28426242]
23. Henderson R, Baldwin JM, Ceska TA, Zemlin F, Beckmann E, Downing KH. 1990. Model for the structure of bacteriorhodopsin based on high-resolution electron cryo-microscopy. *J. Mol. Biol* 213:899–929 [PubMed: 2359127]
24. Schmidt-Krey I 2007. Electron crystallography of membrane proteins: two-dimensional crystallization and screening by electron microscopy. *Methods* 41:417–26 [PubMed: 17367714]
25. Nannenga BL, Shi D, Leslie AGW, Gonen T. 2014. High-resolution structure determination by continuous rotation data collection in MicroED. *Nat. Methods* 11:927–30 [PubMed: 25086503]
26. De Rosier DJ, Klug A. 1968. Reconstruction of three dimensional fiber structures from orthogonal projections. *Nature* 217:130–34 [PubMed: 23610788]
27. Van Heel M 1981. Use of multivariate statistics in analysing the images of biological macromolecules. *Ultramicroscopy* 6:187–94 [PubMed: 7268930]
28. Frank J. 1984. The role of multivariate image analysis in solving the architecture of the limulus polyphemus hemocyanin molecule. *Ultramicroscopy* 13:153–64 [PubMed: 6474597]
29. Frank J, Wagenknecht T, McEwen BF, Marko M, Hsieh CE, Mannella C. 2002. Three-dimensional imaging of biological complexity. *J. Struct. Biol* 138:85–91 [PubMed: 12160704]
30. Scheres SHW, Gao H, Valle M, Herman GT, Eggermont PPB, et al. 2007. Disentangling conformational states of macromolecules in 3D-EM through likelihood optimization. *Nat. Methods* 4:27–29 [PubMed: 17179934]
31. Frank J, Goldfarb W, Eisenberg D, Baker TS. 1978. Reconstruction of glutamine synthetase using computer averaging. *Ultramicroscopy* 3:283–90 [PubMed: 32653]
32. Frank J. 2012. Intermediate states during mRNA-tRNA translocation. *Curr. Opin. Struct. Biol* 22:778–85 [PubMed: 22906732]
33. Henderson R 1995. The potential and limitations of neutrons, electrons and X-rays for atomic resolution microscopy of unstained biological molecules. *Q. Rev. Biophys* 28:171–93 [PubMed: 7568675]
34. Herzik MA, Wu M, Lander GC. 2019. High-resolution structure determination of sub-100 kDa complexes using conventional cryo-EM. *Nat. Commun* 10:1032 [PubMed: 30833564]
35. Gonen S, Akiyoshi B, Iadanza MG, Shi D, Duggan N, et al. 2012. The structure of purified kinetochores reveals multiple microtubule-attachment sites. *Nat. Struct. Mol. Biol* 19:225–30
36. Liu Y, Gonen S, Gonen T, Yeates TO. 2018. Near-atomic cryo-EM imaging of a small protein displayed on a designed scaffolding system. *PNAS* 115:3362–67 [PubMed: 29507202]
37. Wisedchaisri G, Reichow SL, Gonen T. 2011. Advances in structural and functional analysis of membrane proteins by electron crystallography. *Structure* 29:1381–93
38. Nannenga BL, Shi D, Hattne J, Reyes FE, Gonen T. 2014. Structure of catalase determined by MicroED. *eLife* 3:e03600 [PubMed: 25303172]

39. Lu C, Reedy M, Erickson HP. 2000. Straight and curved conformations of FtsZ are regulated by GTP hydrolysis. *J. Bacteriol* 182:164–70 [PubMed: 10613876]
40. Li Z, Trimble MJ, Brun YV, Jensen GJ. 2007. The structure of FtsZ filaments in vivo suggests a force-generating role in cell division. *EMBO J.* 26:4694–708 [PubMed: 17948052]
41. Komeili A, Li Z, Newman DK, Jensen GJ. 2006. Magnetosomes are cell membrane invaginations organized by the actin-like protein MamK. *Science* 311:242–46 [PubMed: 16373532]
42. Medalia O, Weber I, Frangakis AS, Nicastrò D, Gerisch G, Baumeister W. 2002. Macromolecular architecture in eukaryotic cells visualized by cryoelectron tomography. *Science* 298:1209–13 [PubMed: 12424373]
43. Heymann JAW, Hayles M, Gestmann I, Giannuzzi LA, Lich B, Subramaniam S. 2006. Site-specific 3D imaging of cells and tissues with a dual beam microscope. *J. Struct. Biol* 155:63–73 [PubMed: 16713294]
44. Hsieh C, Schmelzer T, Kishchenko G, Wagenknecht T, Marko M. 2014. Practical workflow for cryo focused-ion-beam milling of tissues and cells for cryo-TEM tomography. *J. Struct. Biol* 185:32–41 [PubMed: 24211822]
45. Zachs T, Schertel A, Medeiros J, Weiss GL, Hugener J, et al. 2020. Fully automated, sequential focused ion beam milling for cryo-electron tomography. *eLife* 9:e52286 [PubMed: 32149604]
46. Hoppe W, Gassmann J, Hunsmann N, Schramm H, Sturn M. 1974. Three-dimensional reconstruction of individual negatively stained yeast fatty-acid synthetase molecules from tilt series in the electron microscope. *Physiol. Chem* 355:1483–87
47. Okumura T, Shoji M, Hisada A, Ominami Y, Ito S, et al. 2018. Electron tomography of whole cultured cells using novel transmission electron imaging technique. *Micron* 104:21–25 [PubMed: 29049927]
48. Irobalieva RN, Martins B, Medalia O. 2016. Cellular structural biology as revealed by cryo-electron tomography. *J. Cell Sci* 129:469–76 [PubMed: 26787742]
49. Doerr A. 2016. Cryo-electron tomography. *Nat. Methods* 14:34
50. Henderson R, Unwin PNT. 1975. Three-dimensional model of purple membrane obtained by electron microscopy. *Nature* 257:28–32 [PubMed: 1161000]
51. Mohraz M, Simpson MV, Smith PR. 1987. The three-dimensional structure of the Na,K-ATPase from electron microscopy. *J. Cell Biol* 105:1–8 [PubMed: 3038922]
52. Hasler L, Heymann JB, Engel A, Kistler J, Walz T. 1998. 2D crystallization of membrane proteins: rationales and examples. *J. Struct. Biol* 121:162–71 [PubMed: 9615435]
53. Lévy D, Mossera G, Lamberta O, Moeck GS, Bald D, Rigauda JL. 1999. Two-dimensional crystallization on lipid layer: a successful approach for membrane proteins. *J. Struct. Biol* 127:44–52 [PubMed: 10479616]
54. Miyazawa A, Fujiyoshi Y, Unwin N. 2003. Structure and gating mechanism of the acetylcholine receptor pore. *Nature* 423:949–55 [PubMed: 12827192]
55. Unger VM, Kumar NM, Gilula NB, Yeager M. 1999. Expression, two-dimensional crystallization, and electron cryo-crystallography of recombinant gap junction membrane channels. *J. Struct. Biol* 128:98–105 [PubMed: 10600564]
56. Grigorieff N, Ceska TA, Downing KH, Baldwin JM, Henderson R. 1996. Electron-crystallographic refinement of the structure of bacteriorhodopsin. *J. Mol. Biol* 259:393–421 [PubMed: 8676377]
57. Kühlbrandt W, Wang DN, Fujiyoshi Y. 1994. Atomic model of plant light-harvesting complex by electron crystallography. *Nature* 367:614–21 [PubMed: 8107845]
58. Jones CG, Martynowycz MW, Hattne J, Fulton TJ, Stoltz BM, et al. 2018. The cryoEM method MicroED as a powerful tool for small molecule structure determination. *ACS Cent. Sci* 4:1587–92 [PubMed: 30555912]
59. Martynowycz MW, Gonen T. 2018. From electron crystallography of 2D crystals to MicroED of 3D crystals. *Curr. Opin. Colloid Interface Sci* 34:9–16 [PubMed: 30166936]
60. Hattne J, Reyes FE, Nannenga BL, Shi D, de la Cruz MJ, et al. 2015. MicroED data collection and processing. *Acta Crystallogr. Sect. A Found. Adv* 71:353–60 [PubMed: 26131894]

61. Henderson R. 1995. The potential and limitations of neutrons, electrons and X-rays for atomic resolution microscopy of unstained biological molecules. *Q. Rev. Biophys* 28:171–93 [PubMed: 7568675]
62. Hirai T, Mitsuoka K, Kidera A, Fujiyoshi Y. 2007. Simulation of charge effects on density maps obtained by high-resolution electron crystallography. *J. Electron. Microsc* 56:131–40
63. Liu S, Gonen T. 2018. MicroED structure of the NaK ion channel reveals a Na⁺ partition process into the selectivity filter. *Commun. Biol* 1:38 [PubMed: 30167468]
64. Yonekura K, Kato K, Ogasawara M, Tomita M, Toyoshima C. 2015. Electron crystallography of ultrathin 3D protein crystals: atomic model with charges. *PNAS* 112:3368–73 [PubMed: 25730881]
65. Shi D, Nannenga BL, de la Cruz MJ, Liu J, Sawtelle S, et al. 2016. The collection of MicroED data for macromolecular crystallography. *Nat. Protoc* 11:895–904 [PubMed: 27077331]
66. Rodriguez JA, Ivanova MI, Sawaya MR, Cascio D, Reyes FE, et al. 2015. Structure of the toxic core of α -synuclein from invisible crystals. *Nature* 525:486–90 [PubMed: 26352473]
67. Kissick DJ, Wanapun D, Simpson GJ. 2011. Second-order nonlinear optical imaging of chiral crystals. *Annu. Rev. Anal. Chem* 4:419–37
68. Stevenson HP, Makhov AM, Calero M, Edwards AL, Zeldin OB, et al. 2014. Use of transmission electron microscopy to identify nanocrystals of challenging protein targets. *PNAS* 111:8470–75 [PubMed: 24872454]
69. Gallagher-Jones M, Glynn C, Boyer DR, Martynowycz MW, Hernandez E, et al. 2018. Sub-ångstrom cryo-EM structure of a prion protofibril reveals a polar clasp. *Nat. Struct. Mol. Biol* 25:131–34 [PubMed: 29335561]
70. Hattne J, Shi D, Glynn C, Zee CT, Gallagher-Jones M, et al. 2018. Analysis of global and site-specific radiation damage in cryo-EM. *Structure* 26:759–766.e4 [PubMed: 29706530]
71. Jones CG, Asay M, Kim LJ, Kleinsasser JF, Saha A, et al. 2019. Characterization of reactive organometallic species via MicroED. *ACS Cent. Sci* 5:1507–13 [PubMed: 31572777]
72. de la Cruz MJ, Hattne J, Shi D, Seidler P, Rodriguez J, et al. 2017. Atomic-resolution structures from fragmented protein crystals with the cryoEM method MicroED. *Nat. Methods* 14:399–402 [PubMed: 28192420]
73. Martynowycz MW, Zhao W, Hattne J, Jensen GJ, Gonen T. 2019. Collection of continuous rotation MicroED data from ion beam-milled crystals of any size. *Structure* 27:545–48 [PubMed: 30661853]
74. Duyvesteyn HME, Kotecha A, Ginn HM, Hecksel CW, Beale EV, et al. 2018. Machining protein microcrystals for structure determination by electron diffraction. *PNAS* 115:9569–73 [PubMed: 30171169]
75. Martynowycz MW, Zhao W, Hattne J, Jensen GJ, Gonen T. 2019. Qualitative analyses of polishing and pre-coating FIB milled crystals for MicroED. *Structure* 27:1594–600 [PubMed: 31422911]
76. Zhou H, Luo Z, Li X. 2019. Using focus ion beam to prepare crystal lamella for electron diffraction. *J. Struct. Biol* 205:59–64 [PubMed: 30794865]
77. Martynowycz M, Glynn C, Miao J, de la Cruz MJ, Hattne J, et al. 2017. MicroED structures from micrometer thick protein crystals. *bioRxiv* 152504. 10.1101/152504
78. Otwinowski Z, Minor W. 1997. Processing of X-ray diffraction data collected in oscillation mode. *Methods Enzymol.* 276:306–15
79. Kabsch W 2010. XDS. *Acta Crystallogr. Sect. D Biol. Crystallogr* 66:125–32 [PubMed: 20124692]
80. Battye TGG, Kontogiannis L, Johnson O, Powell HR, Leslie AGW. 2011. iMOSFLM: a new graphical interface for diffraction-image processing with MOSFLM. *Acta Crystallogr. Sect. D Biol. Crystallogr* 67:271–81 [PubMed: 21460445]
81. Parkhurst JM, Winter G, Waterman DG, Fuentes-Montero L, Gildea RJ, et al. 2016. Robust background modelling in *DIALS*. *J. Appl. Crystallogr* 49:1912–21 [PubMed: 27980508]
82. Sheldrick GM. 2015. SHELXT—integrated space-group and crystal-structure determination. *Acta Crystallogr. Sect. A Found. Crystallogr* 71:3–8
83. McCoy AJ, Grosse-Kunstleve RW, Adams PD, Winn MD, Storoni LC, Read RJ. 2007. Phaser crystallographic software. *J. Appl. Crystallogr* 40:658–74 [PubMed: 19461840]

84. Kamegawa A, Hiroaki Y, Tani K, Fujiyoshi Y. 2016. Two-dimensional crystal structure of aquaporin-4 bound to the inhibitor acetazolamide. *Reprod. Syst. Sex. Disord* 65:177–84
85. Oshima A 2017. Structure of an innexin gap junction channel and cryo-EM sample preparation. *Microscopy* 66:371–79 [PubMed: 29036409]
86. Nederlof I, Li YW, Van Heel M, Abrahams JP 2013. Imaging protein three-dimensional nanocrystals with cryo-EM. *Acta Crystallogr. Sect. D Biol. Crystallogr* 69:852–59 [PubMed: 23633595]
87. van Genderen E, Li YW, Nederlof I, Abrahams JP. 2018. Lattice filter for processing image data of three-dimensional protein nanocrystals. *Int. J. Dermatol* 57:34–39 [PubMed: 29090462]
88. Rodríguez DD, Grosse C, Himmel S, González C, De Ilarduya IM, et al. 2009. Crystallographic ab initio protein structure solution below atomic resolution. *Nat. Methods* 6:651–53 [PubMed: 19684596]
89. Martynowycz MW, Hattne J, Gonen T. 2020. Experimental phasing of MicroED data using radiation damage. *Structure* 28:458–464.e2 [PubMed: 32023481]
90. Kupitz C, Grotjohann I, Conrad CE, Roy-Chowdhury S, Fromme R, Fromme P 2014. Microcrystallization techniques for serial femtosecond crystallography using photosystem II from *Thermosynechococcus elongatus* as a model system. *Philos. Trans. R. Soc. B* 369:20130316
91. Sawaya MR, Rodriguez J, Cascio D, Collazo MJ, Shi D, et al. 2016. Ab initio structure determination from prion nanocrystals at atomic resolution by MicroED. *PNAS* 113:11232–36 [PubMed: 27647903]
92. Martynowycz MW, Gonen T. 2021. Efficient, high-throughput ligand incorporation into protein microcrystals by on-grid soaking. *Structure* 29(1):88–95 [PubMed: 33007196]
93. Kunde T, Schmidt BM. 2019. Microcrystal electron diffraction (MicroED) for small-molecule structure determination. *Angew. Chem. Int. Ed* 58:666–68
94. Gruene T, Wennmacher YTC, Zaubitzer C, Holstein JJ, Heidler J, et al. 2018. Rapid structure determination of microcrystalline molecular compounds using electron diffraction. *Angew. Chem. Int. Ed* 57:16313–17
95. van Genderen E, Clabbers MTB, Das PP, Stewart A, Nederlof I, et al. 2018. Ab initio structure determination of nanocrystals of organic pharmaceutical compounds by electron diffraction at room temperature using a Timepix quantum area direct electron detector. *Acta Crystallogr. Sect. A Found. Adv* 74:236–42
96. Matsufuji H, Ichiyama T, Isumi H, Furukawa S. 2005. Low-dose carbamazepine therapy for benign infantile convulsions. *Brain Dev.* 27:554–57 [PubMed: 16310589]
97. Hirschfeld RMA, Kasper S. 2004. A review of the evidence for carbamazepine and oxcarbazepine in the treatment of bipolar disorder. *Int. J. Neuropsychopharmacol* 7:507–22 [PubMed: 15458610]
98. Koytchev R, Vlahov V, Bacratheva N, Giesel B, Gawronska-Szklarz B, et al. 2003. Evaluation of the efficacy of a combined formulation (Grippostad®-C) in the therapy of symptoms of common cold: a randomized, double-blind, multicenter trial. *Int. J. Clin. Pharmacol. Ther* 41:114–25 [PubMed: 12665160]
99. Beck T, Da Cunha CE, Sheldrick GM. 2009. How to get the magic triangle and the MAD triangle into your protein crystal. *Acta Crystallogr. Sect. F Struct. Biol. Cryst. Commun* 65:1068–70
100. Geremia S, Campagnolo M, Demitri N, Johnson LN. 2006. Simulation of diffusion time of small molecules in protein crystals. *Structure* 14:393–400 [PubMed: 16531224]
101. Gonen T, Sliz P, Kistler J, Cheng Y, Walz T. 2004. Aquaporin-0 membrane junctions reveal the structure of a closed water pore. *Nature* 429:193–97 [PubMed: 15141214]
102. Oshima A, Tani K, Hiroaki Y, Fujiyoshi Y, Sosinsky GE. 2008. Projection structure of a N-terminal deletion mutant of connexin 26 channel with decreased central pore density. *Cell Commun. Adhes* 15:85–93 [PubMed: 18649181]
103. Morikawa M, Derynck R, Miyazono K. 2016. TGF- β and the TGF- β family: context-dependent roles in cell and tissue physiology. *Cold Spring Harb. Perspect. Biol* 8:1–24
104. Purdy MD, Shi D, Chrustowicz J, Hattne J, Gonen T, Yeager M. 2018. MicroED structures of HIV-1 Gag CTD-SP1 reveal binding interactions with the maturation inhibitor bevirimat. *PNAS* 115:13258–63 [PubMed: 30530702]

105. Auluck PK, Caraveo G, Lindquist S. 2010. α -Synuclein: membrane interactions and toxicity in Parkinson's disease. *Annu. Rev. Cell Dev. Biol* 26:211–33 [PubMed: 20500090]
106. Sundquist WI, Krausslich HG. 2012. HIV-1 assembly, budding, and maturation. *Cold Spring Harb. Perspect. Med* 2:a006924 [PubMed: 22762019]
107. Lee SK, Potempa M, Swanstrom R. 2012. The choreography of HIV-1 proteolytic processing and virion assembly. *J. Biol. Chem* 287:40867–74 [PubMed: 23043111]
108. Martin DE, Salzwedel K, Allaway GP. 2008. Bevirimat: a novel maturation inhibitor for the treatment of HIV-1 infection. *Antivir. Chem. Chemother* 19:107–13 [PubMed: 19024627]
109. Wainwright M. 2000. Methylene blue derivatives—suitable photoantimicrobials for blood product disinfection? *Int. J. Antimicrob. Agents* 16:381–94 [PubMed: 11118846]
110. Ting CP, Michael A, Funk MA, Halaby SL, Zhang Z, et al. 2019. Use of a scaffold peptide in the biosynthesis of amino acid-derived natural products. *Science* 365:280–84 [PubMed: 31320540]
111. Dick M, Sarai NS, Martynowycz MW, Gonen T, Arnold FH. 2019. Tailoring tryptophan synthase TrpB for selective quaternary carbon bond formation. *J. Am. Chem. Soc* 141:19817–22 [PubMed: 31747522]
112. Qin J, Yang L, Sheng X, Sa Z, Huang T, et al. 2018. Antitumor effects of brucine immunonanoparticles on hepatocellular carcinoma in vivo. *Oncol. Lett* 15:6137–46 [PubMed: 29731843]
113. Arnisona PG, Bibb MJ, Bierbaum G, Bowers AA, Bugni TS, et al. 2014. Ribosomally synthesized and post-translationally modified peptide natural products: overview and recommendations for a universal nomenclature. *Nat. Prod. Rep* 30:108–60
114. Kutscher AH, Seguin L, Zegarelli EV, Piro JD. 1959. Antimicrobial activity of thiostrepton: tube dilution studies. *J. Am. Dent. Assoc* 59:715–20 [PubMed: 14412974]
115. Anderson B, Hodgkin DC, Viswamitra MA. 1970. The structure of thiostrepton. *Nature* 225:233–35 [PubMed: 5409975]
116. Arrebola E, Cazorla FM, Perez-García A, de Vicente A. 2011. Chemical and metabolic aspects of antimetabolite toxins produced by *Pseudomonas syringae* pathovars. *Toxins* 3:1089–110 [PubMed: 22069758]
117. Garman EF, Weik M. 2017. X-ray radiation damage to biological macromolecules: further insights. *J. Synchrotron Radiat* 24:1–6 [PubMed: 28009541]
118. Blake CCF, Phillips DC. 1962. Biological effects of ionizing radiation at the molecular level. *Proc. Ser. Int. At. Energy Agency 92-0-010762-1*, Int. At. Energy Agency, Vienna
119. Hendrickson WA. 1976. Radiation damage in protein crystallography. *J. Mol. Biol* 106:889–93 [PubMed: 978739]
120. Ravelli RBG, Theveneau P, McSweeney S, Caffrey M. 2002. Unit-cell volume change as a metric of radiation damage in crystals of macromolecules. *J. Synchrotron Radiat* 9:355–60 [PubMed: 12409622]
121. Kmetko J, Husseini NS, Naides M, Kalinin Y, Thorne RE. 2006. Quantifying X-ray radiation damage in protein crystals at cryogenic temperatures. *Acta Crystallogr. Sect. D Biol. Crystallogr* 62:1030–38 [PubMed: 16929104]
122. Weik M, Ravelli RBG, Kryger G, McSweeney S, Raves ML, et al. 2000. Specific chemical and structural damage to proteins produced by synchrotron radiation. *PNAS* 97:623–28 [PubMed: 10639129]
123. Karuppasamy M, Karimi Nejadasl F, Vulovic M, Koster AJ, Ravelli RBG. 2011. Radiation damage in single-particle cryo-electron microscopy: effects of dose and dose rate. *J. Synchrotron Radiat* 18:398–412 [PubMed: 21525648]
124. Hattne J, Martynowycz MW, Penczek PA, Gonen T. 2019. MicroED with the Falcon III direct electron detector. *IUCrJ* 6:921–26
125. Taylor G. 2003. The phase problem. *Acta Crystallogr. Sect. D Biol. Crystallogr* 59:1881–90 [PubMed: 14573942]
126. Evans P, McCoy A. 2007. An introduction to molecular replacement. *Acta Crystallogr. Sect. D Biol. Crystallogr* 64:1–10 [PubMed: 18094461]
127. Schenk H. 1984. *An Introduction to Direct Methods. The Most Important Phase Relationships and Their Application in Solving the Phase Problem*. Cardiff, Wales: Univ. Cardiff Press

128. Zubeita C, Nanao M. 2016. Practical radiation damage–induced phasing. *Methods Mol. Biol* 1320:205–18 [PubMed: 26227045]
129. Drenth J. 1999. The solution of the phase problem by the isomorphous replacement method. In *Principles of Protein X-ray Crystallography*, pp. 129–79. New York: Springer

Author Manuscript

Author Manuscript

Author Manuscript

Author Manuscript

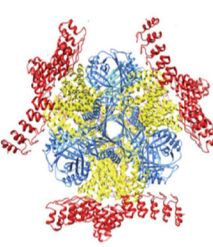
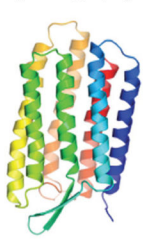
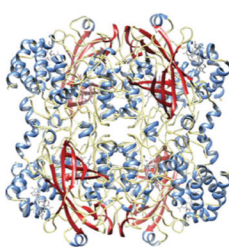
CryoEM techniques	a Tomography 	b Single-particle analysis 	c 2D electron crystallography 	d MicroED 
Advantages	Samples in near native states	High resolution	Samples in lipid bilayer	High resolution from small crystals
Challenges	Typically low (~10 Å) resolution	Molecular weight limit >40 kDa	Requires 2D crystal growth	Requires 3D crystal growth

Figure 1.

The four modalities of cryo-electron microscopy (cryo-EM). (a) A model of the kinetochore assembly by tomography. Panel adapted from Reference 35 with permission from the American Association for the Advancement of Science (AAAS). (b) Structure of a 17-kDa protein, DARPIn, on a scaffold by single-particle analysis. Panel adapted from Reference 36 with permission from AAAS. (c) The structure of bacteriorhodopsin determined by electron crystallography of two-dimensional (2D) crystals. Panel adapted with permission from Reference 37. (d) The structure of catalase determined by microcrystal electron diffraction (MicroED) of 3D crystals. Panel adapted with permission from Reference 38.

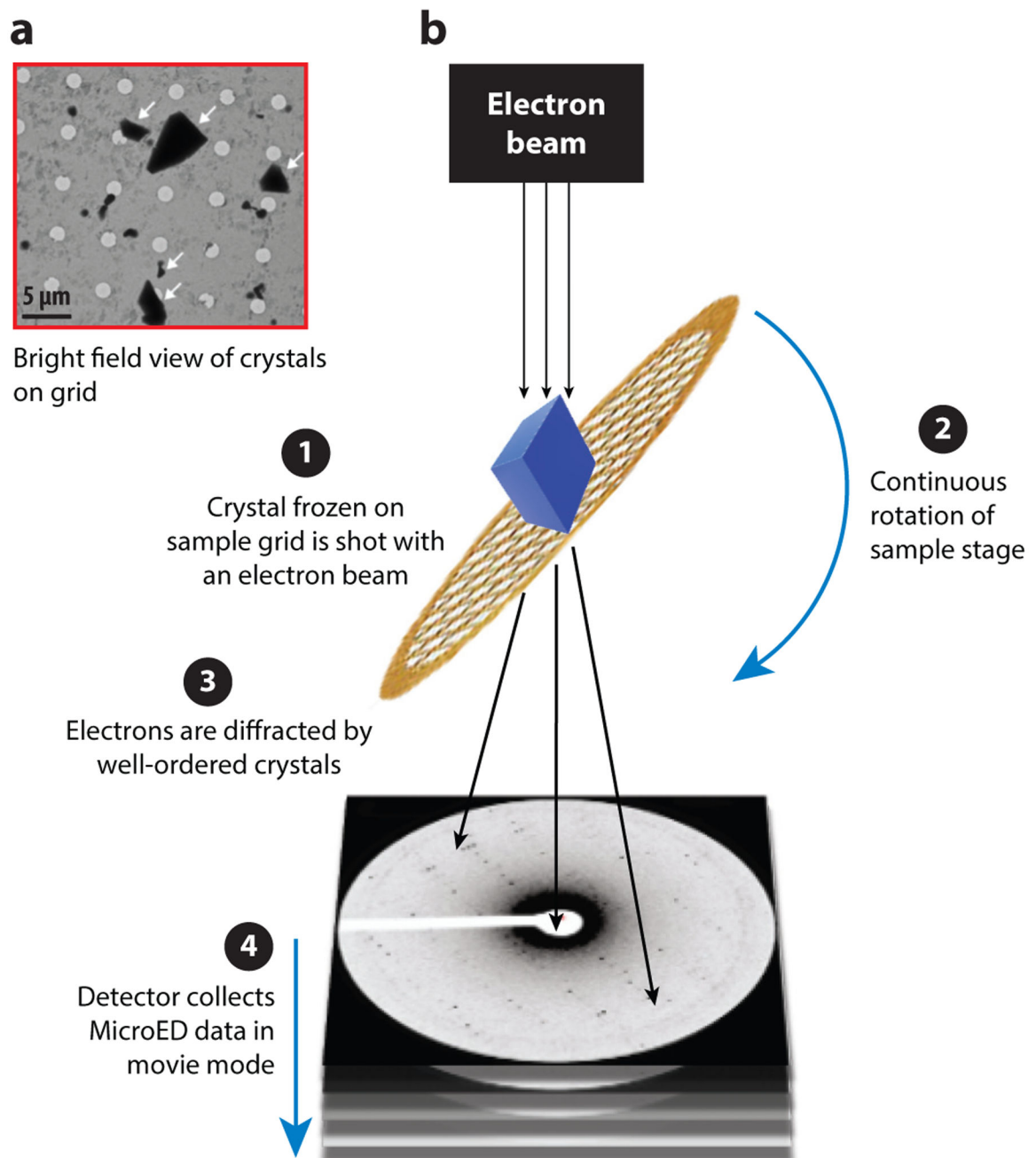
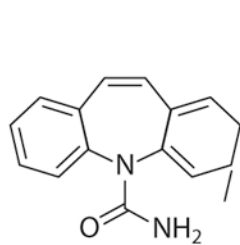
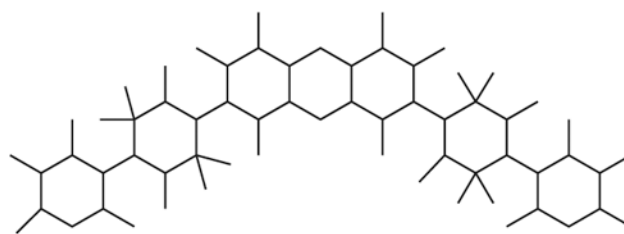
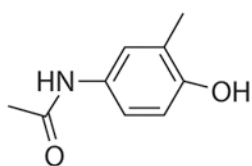


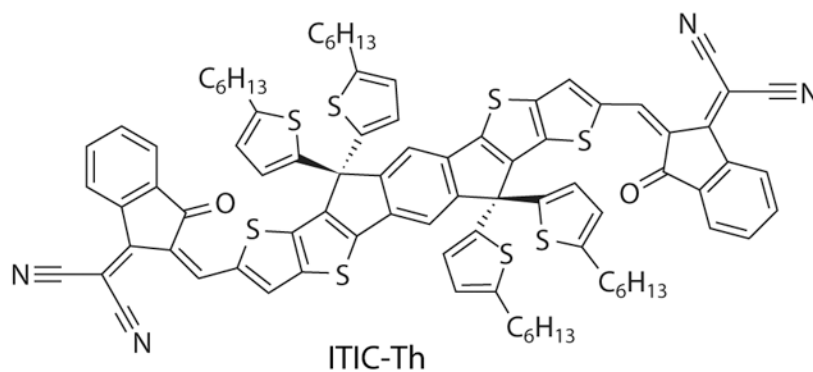
Figure 2. An overview of microcrystal electron diffraction (MicroED). (a) An image of an electron microscope grid in bright field during screening for microcrystals. (b) Once located, a microcrystal is exposed to an electron beam in diffraction mode while being continuously rotated on the sample stage. The diffraction data are then collected as a movie using a fast camera.



Carbamazepine

MBBF₄

Gripostad



ITIC-Th

Figure 3. Examples of structures of small-molecule chemical compounds solved by microcrystal electron diffraction (MicroED). Structures of carbamazepine, MBBF₄, Gripostad, and ITIC-Th are shown.

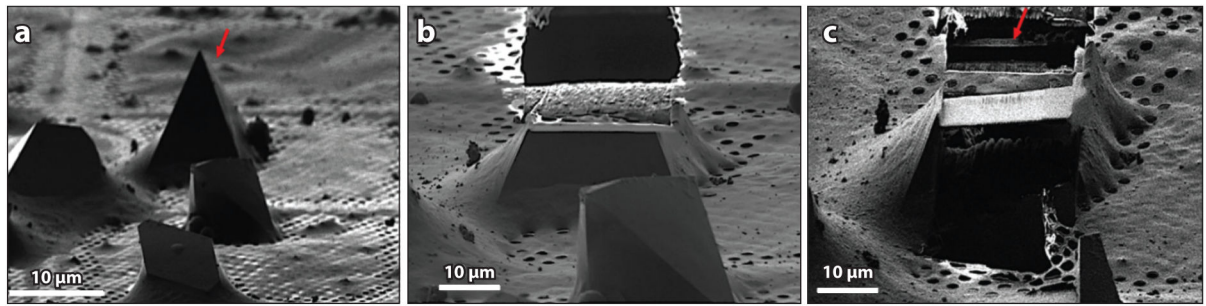
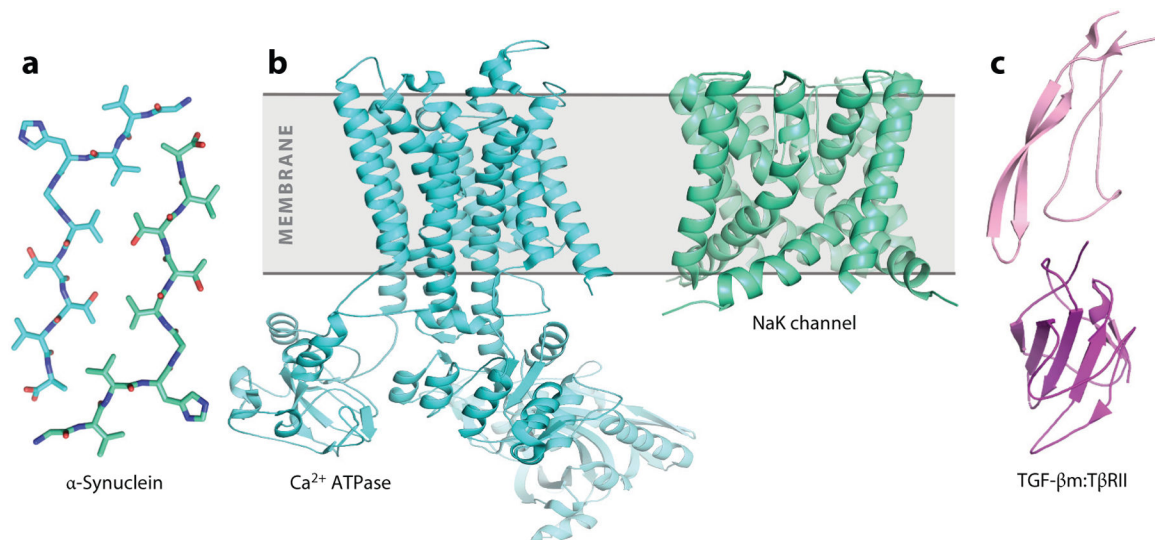


Figure 4. Focused ion beam (FIB) milling of crystals for microcrystal electron diffraction (MicroED). (a) Image of select proteinase K crystals at high magnification before milling. The arrow indicates the crystal that was milled in panel c. (b) FIB image of select crystal from panel a after milling the top of the crystal. (c) FIB image of crystal after milling and cleaning both the top and bottom of the crystal, leaving a lamella indicated by an arrow. Figure reproduced with permission from Reference 73.

**Figure 5.**

Examples of protein structures solved by MicroED that were challenging by other techniques. (a) Structure of α -synuclein NACore (66) (PDB ID: 4ZNN). (b) MicroED structures of the membrane proteins rendered as cyan and green ribbons for Ca^{2+} ATPase (PDB ID: 3J7T/U) (64) and NaK (PDB ID: 6CPV) (63), respectively. (c) MicroED structure of the TGF- β m:T β RII protein-protein complex (PDB ID: 5TY4) (72). Protein rendered as pink and magenta ribbons for TGF- β m and T β RII, respectively. Abbreviations: MicroED, microcrystal electron diffraction; PDB ID, Protein Data Bank identifier.

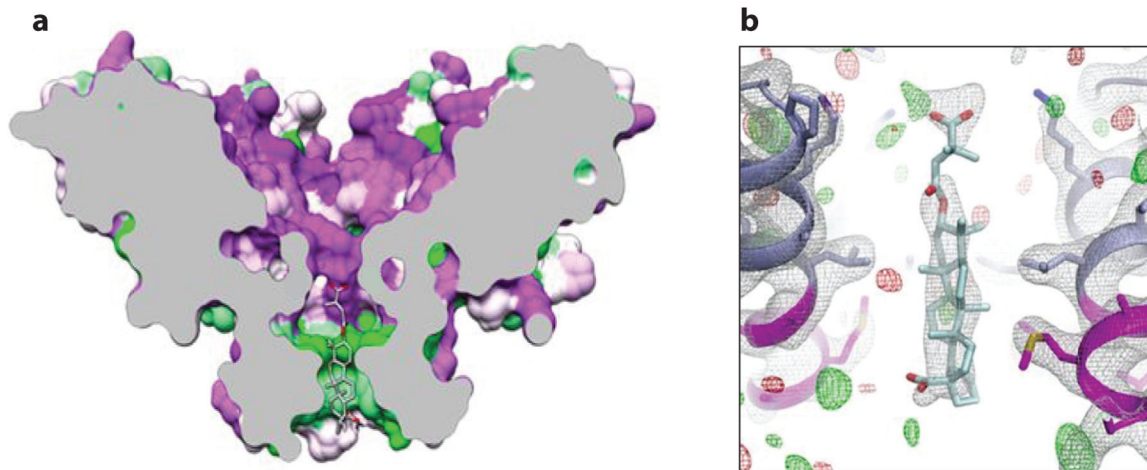


Figure 6. The structure of the HIV GAG-bevirimat complex solved by microcrystal electron diffraction (MicroED) (104). (a) Overall architecture of HIV GAG-bevirimat complex. (b) Expanded view of the bevirimat binding site in the pore of HIV GAG. Both panels reproduced with permission from Reference 104.

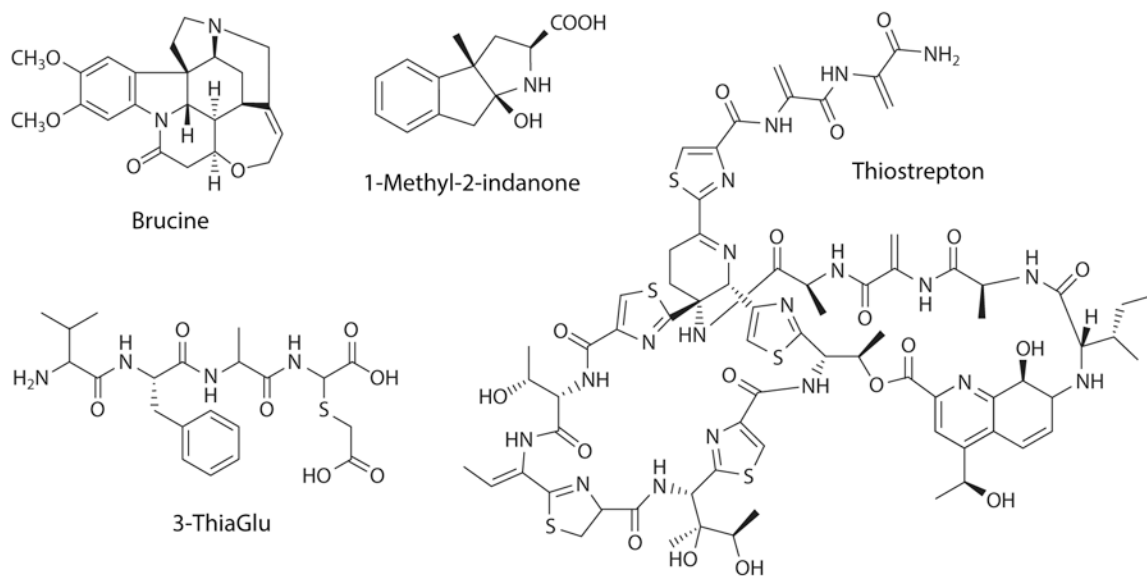


Figure 7. Brucine, 1-methyl-2-indanone, thiostrepton, and 3-thiaGlu are examples of natural products with structures determined by microcrystal electron diffraction (MicroED).

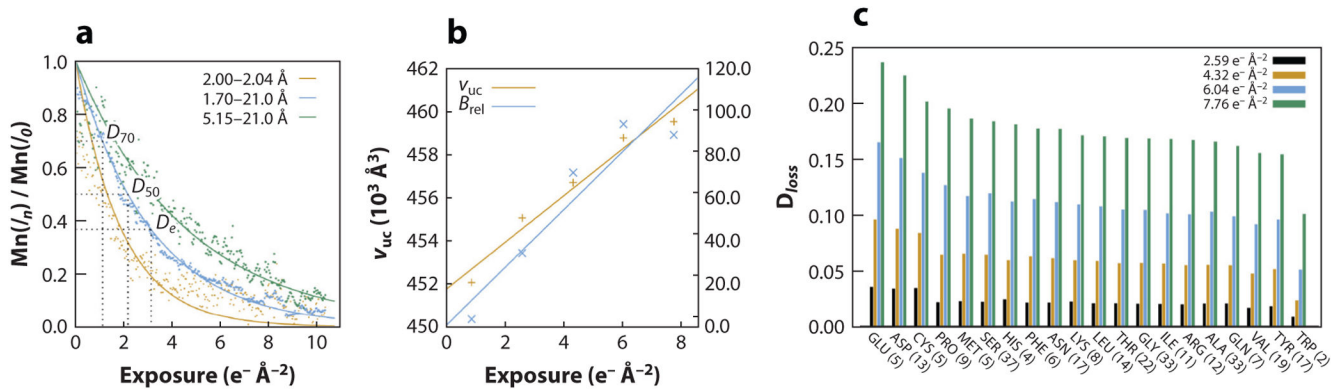


Figure 8. Radiation damage in microcrystal electron diffraction (MicroED) (70). (a) Proteinase K recorded at various exposure rates. (b) Volume and B-factor were averaged across all the crystals at each exposure for proteinase K. (c) Density loss in arbitrary units for all the amino acids, ligands, and ions present in the refined models of proteinase K. All panels adapted with permission from Reference 70.

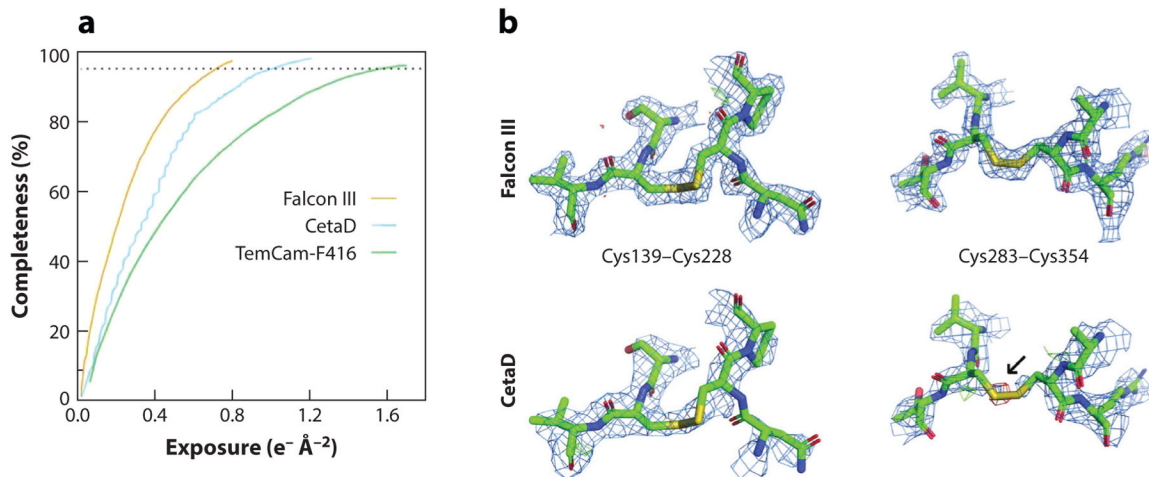


Figure 9.

Expanding the use of direct electron detectors and mitigating radiation damage in microcrystal electron diffraction (MicroED) (124). (a) The exposure dependency of the completeness of proteinase K. The dotted horizontal line marks 95% completeness. (b) The density around the two disulfide bonds for the considered cameras for proteinase K. Both panels adapted with permission from Reference 124.

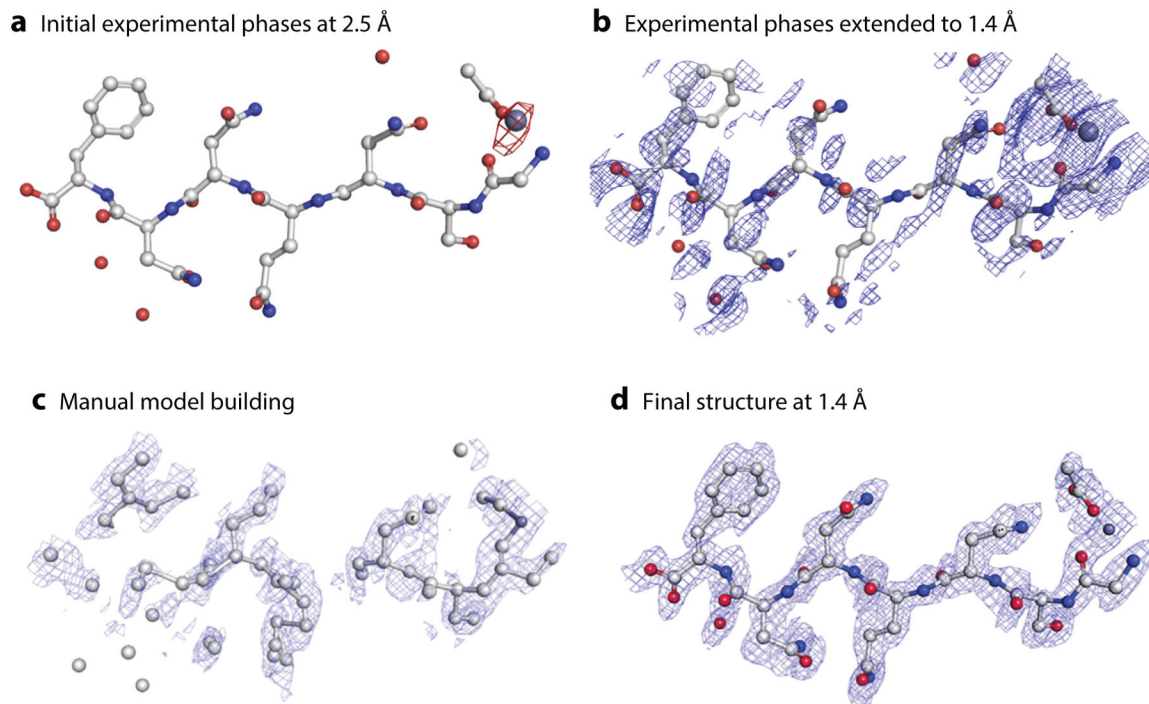


Figure 10.

Identification of heavy metal site and model building by radiation-induced damage for phasing. (a) Fourier difference maps between the damaged and undamaged structure of GSNQNNF using the phases of 6CLI at 2.5 Å resolution contoured at 3σ level. (b) The map using the initial phases extended to 1.4 Å resolution. (c) Density maps at 1.0σ contour for intermediate building steps. (d) The final structure. All panels adapted with permission from Reference 89.